WIS-77/33-Ph
November 1977

PRODUCTION OF SLOW PROTONS IN THE INCLUSIVE REACTIONS $p(\pi^+)+n \rightarrow p_{slow} + x$ AT 195 GeV/c(*)

Y. Eisenberg, B. Haber, D. Hochman, U. Karshon, L. Lyons(†),
E.E.Ronat, A. Shapira, M. Tabak and G. Yekutieli
Weizmann Institute of Science, Rehovot, Israel

and

H. Braun, F. Etienne, A. Fridman, J.P. Gerber, E. Jegham,
H. Johnstad, P. Juillot, G. Maurer and C. Voltolini
Centre de Recherches Nucleaires, Strasbourg, France

Publ. in Nucl. Phys.
B 135: 189, 1978

Abstract

The inclusive reactions $pn \rightarrow p_s+x$ and $\pi^+n \rightarrow p_s+x$ at incident momentum of 195 GeV/c have been studied in an exposure of the Fermilab 30-in.deuterium filled bubble chamber to a mixed (π^+,p) beam. Analysing the t and M^2 dependence of our data within the framework of triple Regge models we conclude that pion exchange yields a dominating contribution. Comparing our data with the pp results we conclude that isoscalar Regge exchange (ω) is much larger than isovector (ρ) Regge exchange . We observe significant leading π^- emission from the recoiling mass x, comparable to that observed in on-mass shell $\pi^-p \rightarrow \pi^-$ experiments. This verifies our conclusions about pion exchange dominance in the above reactions.

1. Introduction

The important role of π-exchange in the inclusive reactions[1]:

$$pp \to p+x \qquad (1)$$

$$pn \to p+x \qquad (2)$$

where x denotes all other particles produced, was stressed by several authors[2-3]. A quantitative evaluation[3] of π, pomeron (P) and resonance (R) exchange contribution to reaction (1) was achieved by fitting the unknown parameters in the triple Regge formulae for the differential cross sections (see eq. (4) below) to about 830 data points from various bubble chamber and counter high energy pp experiments. The validity of these results can be tested by their application to $pn \to p+x$. For this reaction P-exchange and the isoscalar part of R do not contribute while the contribution of π-exchange and isovector R are, by isospin considerations, twice their contribution to $pp \to p+x$. Another reaction in which charge is exchanged is $pp \to \Delta^{++}+x$ which is however more difficult to study experimentally[4].

In this paper we present cross sections for reaction (2) and for the reaction

$$\pi^+ n \to p+x \qquad (3)$$

at 195 GeV/c. Since this energy is sufficiently high for triple Regge analysis to be adequate we compare our results with the prediction of ref. (3). Our experimental procedures are described in section 2. In section 3 we compare our data with the theoretical predictions and try to deduce the dominating exchanges in reactions (2) and (3). In section 4 we present and discuss leading π^- effects in the recoiling mass against the slow proton, and in section 5 we summarize our conclusions.

2. Experimental procedure and cross sections

Our data are taken from about 70,000 pictures obtained in an exposure of the Fermilab 30 inch deuterium filled bubble chamber and proportional wire hybrid system to a positive π^+/p beam of 195 GeV/c. A detailed description of the experimental set-up can be found in ref. (5). An upstream Čerenkov counter determined the mass of the interacting particles. It was found that about 67% of the events were due to protons and about 28% due to pions.

All the film was scanned at least twice, with an efficiency of ∿98% for three and more outgoing charged particles. The overall efficiently[6] for inelastic one or two prongs is poor, however finding such events having only a slow outgoing dark proton is relatively easy. All outgoing tracks were measured and those which failed were remeasured. Thus all our events are complete and charged balanced. Reconstructed positive tracks having laboratory momentum $P_{LAB}<1.4$ GeV/c were identified as protons or pions by ionization. We select pure samples of neutron interactions by choosing events having either odd prongs or even prongs with a backward spectator in the laboratory system. With this procedure we have obtained 470 $pn \to p_s+x$ events and 199 $\pi^+ n \to p_s+x$ events, all having a visible slow proton momentum $p_s<1.4$ GeV/c.

Several corrections were applied to the raw data. These include corrections for secondary scatters near the vertex, double scattering in the deuteron, losses of various kinds, etc. Most of these corrections

were discussed earlier[6,7] and were used to derive multiplicities. For cross section derivation we have defined a weight $\omega(n) = \sigma(n)/N(n)$ for each multiplicity n, where $\sigma(n)$ is the corrected multiplicity cross section and N(n) the number of events of the same multiplicity in our data. The slow proton cross-section σ_s was then derived from $\sigma_s = \sum_n \sigma_s(n) = \sum_n N_s(n) \cdot \omega(n)$ where $N_s(n)$ is the number of events of multiplicity n having a visible slow proton.

The fraction $F(n)[= N_s(n)/N(n)]$ of slow proton events (for $|t| \leq 1.4$ GeV^2 which corresponds to our P_s cut) to all events of multiplicity n for $pn \to p_s + x$ at 195 GeV/c is plotted in Fig.(1a). The value F(1) was obtained indirectly by normalizing the observed $N_s(1)$ (two events), to $N_s(3)$ (105 events) and using the corresponding topological cross-sections[6]. We find $F(1) = (1.3 \pm 0.9)\%$ and $\sigma_s(1) = (0.02 \pm 0.014)$ mb, which is in agreement with Ref.(1b) for $pn \to p_s + x$ at 100 GeV/c. The slow proton cross sections $\sigma_s(n)$ are plotted in Fig.(1b). In Figs.(1a) and (1b) we also plot the corresponding values for $pp \to p_s + x$ at 205 GeV/c[8]. The most striking difference between the two reactions occurs in the low multiplicities and is due to the diffractive component in the pp reactions. At the very highest multiplicities the distributions merge one into the other. The higher P_s yield in the proton reactions between 6-12 prongs, where the diffractive component is small, may be due to non-diffractive fragmentation of the target nucleon[7].

The overall inclusive slow proton cross sections σ_s at 195 GeV/c for reactions (2) and (3) are given in Table I for several $|t|$ or P_{Lab} cuts. A comparison with σ_s for reaction (2) at other energies (same cuts) shows that σ_s is fairly constant with energy. The ratio $\sigma_s(\pi^+ n \to p_s + x)/\sigma_s(pn \to p_s + x)$ for $|t| < 1.4$ GeV is 0.66 ± 0.06 (in agreement with the ratio 0.68 ± 0.06 found at 100 GeV/c[1b]) and equals $\sigma_{inel}(\pi^+ n)/\sigma_{inel}(pn)$ (= 0.645) within errors. This shows that indeed target fragmentation governs the inclusive slow proton emission in both reactions[7], providing vertex factorization holds.

Most of the kinematic quantities (like S, t, M^2, etc.) depend on the target momentum which, due to the Fermi motion, is not unique for all events. For events with a visible spectator the target 4-vector n was taken to be $n = d - p_{spec}$ where, d and p_{spec} are the deuteron and proton spectator 4-vectors respectively. For events with an invisible spectator the target neutron 3-momentum was assumed to be zero but its total energy included the average kinetic energy due to the Fermi motion of the neutron. The smearing in the kinematic variables (M^2, t, etc.) due to this procedure causes only a small shift in their average[1c] values. The resulting dispersion is larger (e.g. full width at half maximum of 30 GeV^2 in M^2), however it does not affect our conclusions since it is smaller or equal to the bin width used in the experimental distributions. It explains in part some of our negative M^2 values.

3. Differential cross sections and triple Regge analysis

The application of triple Regge formalism (Fig. 2) to reactions (1) and (2) yields the following expression for the differential cross sections[3]:

$$S \frac{d\sigma}{dM^2 dt} = \frac{1}{S} \sum_{ijk} G_{ijk}(t) \left(\frac{S}{M^2}\right)^{\alpha_i(t)+\alpha_j(t)} (M^2)^{\alpha_k(0)} \qquad (4)$$

where, $\sqrt{S}$, t and M^2 are the overall CM energy, the momentum transfer between a and c and the squared mass of the system x respectively. Eq. (4) represents a sum over all possible exchanged trajectories

i, j, k in Fig. (2b) and should be valid for $M^2 \ll S$ and not for too small M^2. First, using the rough approximation: $\alpha_P=1.0$, $\alpha_\pi=0$ and $\alpha_R = 0.5$ where P, π and R denote the pomeron, pion and resonance trajectories, and integrating over t we get:

$$\frac{d\sigma}{dM^2}(PPP) \approx \frac{1}{M^2} \quad ; \quad \frac{d\sigma}{dM^2}(RRP) \approx \text{const} \quad \text{and} \quad \frac{d\sigma}{dM^2}(\pi\pi P) \approx M^2 \,. \qquad (4a)$$

In Fig. 3 we have plotted $S\,\frac{d\sigma}{dM^2}$ as a function of M^2/S for $pn \to p_s+x$ at 195 (this experiment) and 11.6 GeV/c[1a]. We note that the data of the two experiments agree with each other and that both are in disagreement with the simple predictions of eq.(4a) for pure PPP or RRP exchange. The depletion of events at small M^2/S indicates a large contribution of π-exchange at both energies.

To be more quantitative we have used the results of ref. (3), where eq. (4) has been fitted to about 830 data points of high energy $pp \to p_s+x$ interactions. Six possible trajectory combinations, PPP, PPR, RRP, RRR, ππP and ππR were considered with $\alpha_P(t) = 1.0+\alpha' t$, $\alpha_R(t) = 0.5+t$ and $\alpha_\pi(t) = 0.0+t$. The $G_{ijk}(t)$ were assumed to have the form $a_1 e^{-b_1 t} + a_2 e^{-b_2 t}$ except for pion exchange where:

$$G_{\pi\pi k}(t) = \frac{1}{4\pi}\,\frac{g^2}{4\pi}\,\sigma^k_{tot}(\pi p)\,\frac{|-t|}{(t-\mu^2)^2}\,e^{b(t-\mu^2)} \quad (k = P \text{ or } R) \qquad (5)$$

and $\sigma^P_{tot}(\pi p)$, $\sigma^R_{tot}(\pi p)$ are pomeron (constant) and resonance ($\sim \frac{1}{\sqrt{S}}$) parts of the $\pi^o p$ total cross sections. The fitted quantities were a_1, a_2, b_1, b_2 for PPP, PPR, RRP, RRR, b in $G_{\pi\pi k}(t)$ and α' in $\alpha_P(t)$. In this fit b=0 was favoured unlike ref. (2) where b=4 GeV^{-2} was used in the π-exchange term (see also ref.4b). The integration of eq.(4) over the part of M^2-t plane used in our experiment ($|t| \leq 1.4\ GeV^2$) yields a contribution of 6.15 mb for π-exchange (∿5.50mb from ππP and ∿0.5mb from ππR) to reaction (2) which is close to our observed cross

section of (6.06 ± 0.28) mb. This would imply that π-exchange alone accounts for our observed cross-sections.

In Figs. (4a) and (4b) we have plotted $S\cdot\frac{d\sigma}{dM^2}$ and $\frac{d\sigma}{dt}$ for reactions (2) and (3), respectively. The curves are the calculated cross-sections for the ππP term (lower curve) and for ππP + ππR (upper curve). In the $S\cdot\frac{d\sigma}{dM^2}$ graph we also show the Bishari calculations[2] (broken curve). We see from Fig.4 that the triple Regge[3] calculations agree with the experimental data for the π^+ and p reactions in both shape and magnitude. In Fig.5 we have plotted $S\cdot\frac{d\sigma}{dt\,dM^2}$ for various t cuts in both this pn experiment and at 11.6 GeV/c[1a]. The curves represent the calculated π-exchange contribution (with b=0) and are in good agreement with experiment (at 200 GeV/c the ππR contribution is only 10% of ππP, thus both contributions are given together). Similar agreement, in a more restricted (t,M^2)-region, was observed in the 100 GeV/c experiment[1b]. For b>0, which cannot be ruled out experimentally, the calculated π-exchange cross-section will be smaller and thus allow a larger contribution of isovector R-exchange (e.g. ρ-exchange) in reaction (2). However, in the next section we present some further evidence for the dominance of π-exchange in reactions (2) and (3) from a study of leading π^- effects in the system x recoiling against the slow proton.

In Fig.6 we compare the M^2 distribution in our experiment at 195 GeV/c with that for $pp \to p+x$ at 205 GeV[8] using the same t-cuts ($|t|<1.4\ GeV^2$) in both experiments. For the higher M^2/S (e.g. $M^2>40\ GeV^2$), where the PPP and PPR contributions are small[3], $(d\sigma(pp)/dM^2)/(d\sigma(pn)/dM^2)$ is about 3/2. Neglecting interference terms we get by isospin considerations $\sigma(pp) = \sigma_0+\sigma_1$ and $\sigma(pn) = 2\sigma_1$

where σ_o and σ_1 are the contributions of isospin zero and one exchanges. Then from the experimental factor $\sigma(pp) = \frac{3}{2}\sigma(pn)$ we get $\sigma_o \approx 2\sigma_1$ which implies that, for a dominating π-exchange in σ_1 for reaction (2), the isoscalar R contribution to reaction (1) is much larger than the isovector R exchanges. This conclusion is in agreement with the fact that $pp\omega^o$ coupling is larger than $pp\rho^o$, for small t (non-spin flip amplitudes), as expected from SU(3).

4. Leading π^- in the MM system

It has been noted before[9] that in reactions initiated by pions and protons there is an enhancement in the inclusive cross-section in the forward direction, for $\pi^{\pm}p \to \pi^{\pm}+x$, $pp \to p+x$. This leading particle effect, when expressed as an invariant cross-section as a function of x, does not depend much on the nature of the beam particle or on the total cms energy S[9]. Similar leading particle effects have also been observed in off mass-shell sub-structures[10]. We have therefore looked for leading π^- effects in the mass recoiling against the proton in reactions (2) and (3) above. This was done in order to understand better the exchange mechanism in these reactions and in particular in order to separate π^- from ρ^- exchange contributions to the slow proton events.

For each event we have made a transformation into the rest system of the recoiling mass against the slow proton, with the collision-axis defined as the usual t-channel direction, namely, the direction of the beam particle and the exchanged particle, whose 4-vector was taken to be that of the target neutron minus the observed slow proton. In this frame of reference we defined the usual Feynman x variable and looked for the inclusive x-distribution of the negative pions. (Positive x

here means emission of the π^- along the exchange direction). One would expect that for a dominating π^- exchange the x distribution of the leading pions at a given M_x^2 region will be similar to that observed (on mass-shell) in π^- initiated reactions with S value similar to the M_x^2 region and in particular, for example, the π^- yield for $x \geq 0.5$ should be similar in both cases. On the other hand, if ρ^- exchange contributes significantly to reactions (2) and (3), the fraction of leading π^-'s at $x \geq 0.5$ should be considerably smaller than that observed in on mass-shell reactions since the available energy would be divided between the π^- and π^o.

Our data is shown in Fig.7 and summarized in table 2, where we also show data of on mass-shell experiments[9,11]. It is quite obvious from our data that the missing mass recoiling against the slow proton in the reactions $pn \to p_{slow}+MM$ and $\pi^+n \to p_{slow}+MM$ shows a very pronounced leading π^- peak* in the region $x \geq 0.5$. The π^- is emitted in the direction of the exchanged charged particle in the above reactions. The normalized invariant cross-section

$$\frac{1}{\sigma_T}F(x) = \frac{1}{\sigma_T}\int \frac{2E}{\pi\sqrt{S}} \frac{d^2\sigma}{dx dp_T^2} dp_T^2 \qquad (6)$$

* We wish to point out that these leading π^-'s in the MM system are responsible for the low mass enhancement of the $M(p_{slow}\pi^-)$ structure reported in our previous publication (ref.7) on the neutron fragmentation in reactions (2) and (3). Analogous effects were reported in ref.10: In studies of the reactions $\pi^-/(p)p \to \Delta^{++}+MM$, the leading π^- in the MM system and the Δ^{++} showed a low mass $M(\Delta^{++}\pi^-)$ enhancement.

which is shown in Fig.7 for our off mass-shell data agrees with that seen in on mass-shell experiments*. A similar agreement has been reported in ref.4d, between the inclusive π^- spectra emitted from the MM system recoiling against the Δ^{++}, in the reaction $pp \to \Delta^{++}+MM$, and the inclusive on mass-shell data $\pi^-p \to \pi^-+x$. Quantitatively, from table 2 we realize that the fraction of π^-'s with $x \geq 0.5$ in our data, for all M^2 intervals, is somewhat larger though consistent with the corresponding fractions observed in on mass-shell experiments. If ρ^- exchange accounts for a considerable fraction of our inclusive p_{slow} spectrum, one would expect the leading particle in the final state to be a ρ^- and thus the integral of eq.(6) for the region $x \geq 0.5$ to be substantially smaller than that observed in on mass-shell data, since the leading particle energy would be divided between the π^- and π^o from the ρ^- decay. The fact that we can observe (see table 2) in all MM^2 regions up to 240 GeV^2 a fraction of π^-'s for $x \geq 0.5$ equal or larger than that observed in on mass-shell $\pi^-p \to \pi^-$ experiments, shows that up to $MM^2 \cong$ 240 GeV^2 pion exchange completely dominates reaction (2). ρ^- exchange is thus excluded at least in the regions of validity of eq.(4) and the conclusions of the previous section are therefore verified. We wish also to point out that we see leading π^- effects in the system x produced in the reaction $\pi^+n \to p_s+x$. However, since for this reaction

* We note that our 3-prong events include also "elastic scattering" of the exchanged particle, "π^-"$p \to \pi^-p$. Thus, for comparison purposes, we added elastic π^-p scattering to the on mass-shell data of Fig.7 and table 2.

comparison with on mass-shell $\pi^+\pi^-$ experiments is impossible, no similar conclusions can be drawn about the domination of π-exchange in reaction (3). Nevertheless, since the size of the leading π^- effect (see table 2) is the same for reactions (2) and (3) and because of the similarity of the two reactions which was discussed in the previous section, one may assume that indeed π-exchange dominates both reactions.

5. Conclusions

We find that the yield of visible slow proton ($P_{LAB} < 1.4$ GeV/c) emission is high in both reactions studied in this experiment, $pn \to p_s+x$ and $\pi^+n \to p_s+x$. The yield (slow protons per inelastic interaction - Fig.1) does not change much with topology and its average is 0.20 ± 0.01 for pn and 0.21 ± 0.02 for π^+n. This is in contrast with the corresponding proton target reaction[8] at our energy, $pp \to p_s+x$, where the low topologies show a very high yield of slow protons due to the contributions of the diffractive component. The ratio of the slow proton cross-section in π^+n to pn is found to be 0.66 ± 0.06, in agreement with that observed[1b] at 100 GeV/c (0.68 ± 0.06), and within errors equals to $\sigma_{inel}(\pi^+n)/\sigma_{inel}(pn)$ (0.645). This indicates that neutron target fragmentation[7] is the primary source of the slow proton emission.

Analyzing our data in terms of the triple Regge Formalism[3], we find that our t and M^2 distributions, as well as the invariant cross-section $S \cdot \frac{d\sigma}{dtdM^2}$ for reactions (2,3) can be well explained by the pion exchange terms $\pi\pi P$ and $\pi\pi R$. This extends the previous results[1a,1b] to much higher t, M^2 regions. However, from this analysis one cannot rule out some isovector R-exchange contributions (RRP) at our energy.

The Feynman x-distribution of the π^-'s emitted from the MM recoiling against the slow proton, shows a remarkable peak near x=1, similar to that observed in π^-p on mass-shell experiments. In particular, we note an equality, or even an excess in the fraction of leading π^-'s (pions having $x \geq 0.5$) in our off mass-shell data as compared with the on mass-shell experiments (see table 2 and Fig.7). This clearly indicates dominance of π exchange in reaction (2) and little or no ρ^- exchange contributions, at least in the region $M^2 \leq 240$ GeV^2.

Finally, comparing our invariant cross sections at the high mass regions ($M^2 > 40$GeV^2) with the $pp \to p_s + x$ results, we note that $\sigma(pp)$ is higher by about a factor of 1.5. Since at the high M^2/S regions the PPP and PPR terms are small[3], the main cross section is due to isoscalar R exchange (ω), and isovector exchange (ρ and π). From our observed experimental cross sections and isospin considerations, we conclude that $\sigma_o \gtrsim 2 \cdot \sigma_1$ and since we know that σ_1 is mostly due to π exchange, we conclude that isoscalar R exchange (ω) contribution to reaction (1) is much larger than isovector exchange (ρ).

We are grateful to the Fermilab staff and the Proportional Wire Hybrid System Consortium for making this experiment possible. We wish to thank our scanning, programming and electronics staff for their efforts and diligence in all the stages of measurements and data processing. The help of E. Koller in the early stages of the experiment is greatly appreciated.

References

*Research was supported by a grant from the United States-Israel Binational Science Foundation (BSF), Jerusalem, Israel.

†Permanent address: Nuclear Physics Laboratory, Oxford, England.

1) Previous experimental studies of $pn \to p+x$ are:
   (a) A. Engler et al., Nucl. Phys. B81 (1974) 397.
   (b) J. Hanlon et al., Phys. Rev. Lett. 37 (1976) 967.
   (c) B. Robinson et al., Phys. Rev. Lett. 34 (1975) 1475.
   (d) J. Engler et al., Nucl. Phys. B84 (1975) 70.

2) M. Bishari, Phys. Lett. 38B (1972) 510.

3) R.D. Fields and G.C. Fox, Nucl. Phys. B80 (1974) 367.

4) Some recent studies of $pp \to \Delta^{++}+x$ are:
   (a) 100 GeV/c: J. Erwin et al., Phys. Rev. Lett. 35 (1975) 980. Preprint UCD-PPL 76-11-01 (1976).
   (b) 200 GeV/c: S.J. Barish et al., Phys. Rev. D5 (1975) 1260.
   (c) 300 GeV/c: F.T. Dao et al., Phys. Rev. Lett. 30 (1973) 34.
   (d) 400 and 102 GeV/c: J.P. De Brion et al., Phys. Rev. Lett. 34 (1975) 910.

5) D. Fong et al., Phys. Lett. 53B (1974) 290; Nucl.Phys.B102(1976)386.

6) Y. Eisenberg et al., Phys. Lett. 60B (1976) 305.

7) Y. Eisenberg et al., Phys. Rev. Lett. 38 (1977) 108.

8) J. Whitmore et al., Phys. Rev. D11 (1975) 3124.

9) J. Whitmore, Phys. Reports (Phys. Lett. C) 27 (1976) 187.

10) J.B. De Brion et al., Phys. Lett. B52 (1974) 477 and reference 4d; D. Brick et al., "Inclusive Δ^{++} Production in π^-p Interactions at 147 GeV/c", submitted to Phys. Rev. D (1977).

11) J.T. Powers et al., Phys. Rev. D8 (1973) 1947.

Table 1: Slow proton cross sections (mb) in reactions (1)-(3)

Reaction / |t| cut	$pn \to p_s + x$			$pp \to p_s + x$	$\pi^+ n \to p_s + x$	
	195 GeV/c	100 GeV/c (ref. 1b)	11.6 GeV/c (ref. 1a)	205 GeV/c (ref. 8)	195 GeV/c	100 GeV/c (ref. 1b)
$\|t\| < 1.4$ GeV^2 or $P_{Lab} < 1.4$ GeV/c	(6.1±0.3)	-	-	(11.33±0.33)	(4.1 ±0.3)	-
$\|t\| < 1.0$ GeV^2 or $P_{Lab} < 1.25$ GeV/c	(5.15±0.25)	(5.7±0.3)	-	-	(3.4 ±0.3)	(3.9±0.3)
$\|t\| < 0.82$ GeV^2 or $P_{Lab} < 1.0$ GeV/c	(4.55±0.25)	-	$(5.1\ ^{+0.4}_{-0.1})$	-	(2.9±0.25)	-

Table 2: The ratio $R = \int_{0.5}^{1.0} F(x)dx / \int_{-1.0}^{0.5} F(x)dx$ in the on mass-shell reaction $\pi^- p \to \pi^- + x$ and in the off mass-shell inclusive reactions "π^-"$p(\pi^+) \to \pi^- + x$.

	On mass-shell[a]			Off mass-shell (this experiment)					
P_{Lab} (GeV/c)	16	40	100	-		-		-	
S or M^2 (GeV^2)	31	76	188	0 - 60		60 - 120		120 - 240	
Initial state	-	-	-	pn	$\pi^+ n$	pn	$\pi^+ n$	pn	$\pi^+ n$
σ_T (mb)	25.1	24.4	24.2	0.88±0.10	0.47±0.10	1.73±0.15	1.21±0.16	3.36±0.22	2.39±0.23
$\int_{0.5}^{1.0} F(x)dx$ (mb)	12.1	10.4	11.7	0.57±0.13	0.25±0.09	0.95±0.17	0.27±0.08	1.71±0.25	0.59±0.12
$\int_{-1.0}^{0.5} F(x)dx$ (mb)	23.8	25.7	25.3	0.81±0.09	0.30±0.05	2.18±0.16	0.86±0.07	4.64±0.21	1.77±0.10
R	0.51	0.40	0.46	0.70±0.18	0.84±0.32	0.44±0.08	0.32±0.09	0.37±0.06	0.33±0.07

(a) Data taken from ref. 9. The errors in the on mass-shell experiments are much smaller than those of the off mass-shell and thus they have been omitted.

Figure Captions

Fig. 1. (a) The ratio F(n) of slow proton events to all events of multiplicity n as a function of n. (b) Slow proton cross-sections vs. n in the reaction $pn \to p_s + x$ at 195 GeV/c for $|t| < 1.4$ GeV^2 (circles). The points are the same quantities for $pp \to p_s + x$ at 205 GeV/c with the same momentum cut (from ref. (8)).

Fig. 2. (a) Feynman diagram for the inclusive process $a+b \to c+x$. (b) The corresponding triple Regge diagram for $a+b \to c+x$. For reaction (2) a is neutron; b and c protons. Indices i,j,k denote the exchanged Regge trajectories.

Fig. 3. $S \frac{d\sigma}{dM^2}$ vs. $\frac{M^2}{S}$ at 195 GeV/c (points) and at 11.6 GeV/c (histogram) for $|t| < 0.8$ GeV^2.

Fig. 4. (a) $S \frac{d\sigma}{dM^2}$ vs. M^2, for $|t| \leq 1.4$ (GeV/c)^2, for the reactions $pn \to p_s + x$ and $\pi^+ n \to p_s + x$ at 195 GeV/c. (b) $\frac{d\sigma}{dt}$ for the above reactions. The curves show the contributions of π exchange ($\pi\pi P$ and the sum $\pi\pi P$ and $\pi\pi R$) and (in (a)) also the Bishari[2] model results (dashed curve),

Fig. 5. $S \frac{d\sigma}{dM^2 dt}$ vs. M^2 for several $|t|$ regions at (a) 195 GeV/c and (b) 11.6 GeV/c[1a]. Curves are discussed in text.

Fig. 6. $S \frac{d\sigma}{dM^2}$ vs. M^2 for $pn \to p_s + x$ at 195 GeV/c and $|t| \leq 1.4$ GeV^2. The dashed line represents the (smoothed) cross-section for $pp \to p_s + x$ at 205 GeV/c with the same t-cut (ref.8).

Fig. 7. The normalized invariant cross-section (eq.6) of inclusive π^- production in the reaction $pn \to p_{slow} + x$, in the rest frame of the system x (solid histogram) compared with inclusive π^-

production in $\pi^- p$ collisions at several energies (dots), corresponding to the various M_x^2 bins used in this experiment. See text for definition of axis. Experimental over-flow ($x > 1.0$) was added to the highest physical bin, $x = 0.9$-1.0. Elastic scattering is included in the data. Error bars are for solid histogram and, when not plotted, are within one s.d. with the corresponding dots.

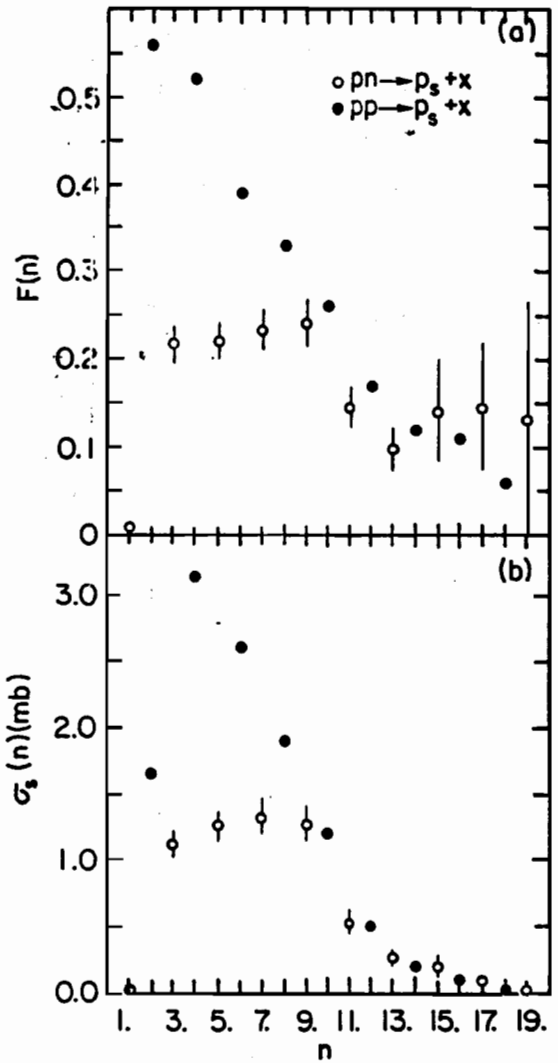
(a)
o pn→p_s+x
• pp→p_s+x
F(n)
0.5
0.4
0.3
0.2
0.1
0
(b)
σ_s (n)(mb)
3.0
2.0
1.0
0.0
1. 3. 5. 7. 9. 11. 13. 15. 17. 19.
n

Fig. 1

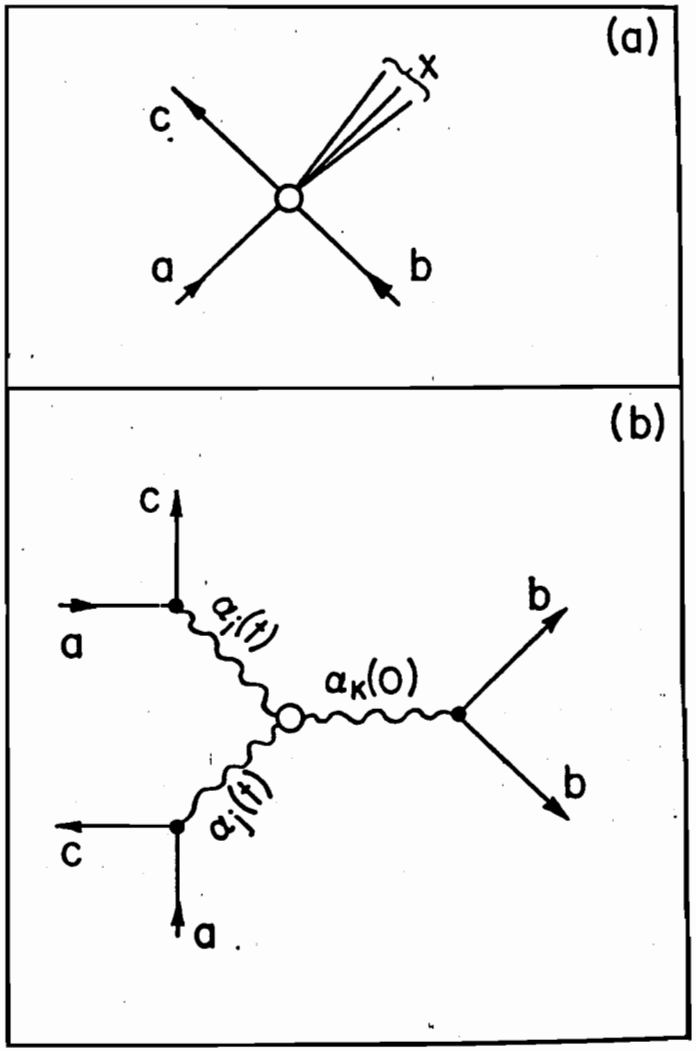
(a)
X
c
a
b
(b)
c
a
b
b
c
a
α_i(t)
α_K(0)
α_j(t)

Fig. 2

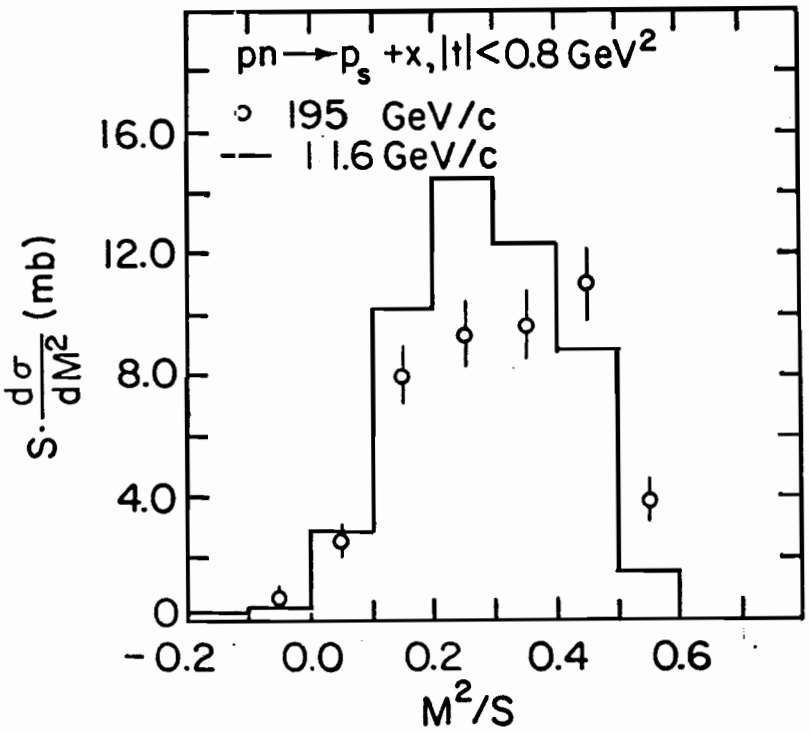
pn → p_s +x, |t|<0.8 GeV²
195 GeV/c
11.6 GeV/c
S·dσ/dM² (mb)
16.0
12.0
8.0
4.0
0
-0.2
0.0
0.2
0.4
0.6
M²/S

Fig. 3

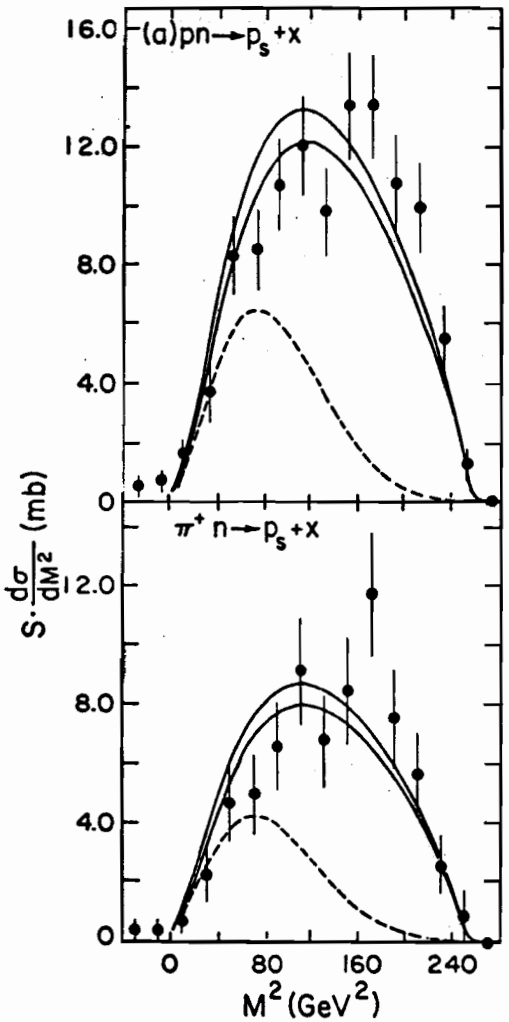
(a) pn → p_s +x
π⁺ n → p_s +x
S·dσ/dM² (mb)
16.0
12.0
8.0
4.0
0
0
80
160
240
M² (GeV²)

Fig. 4a

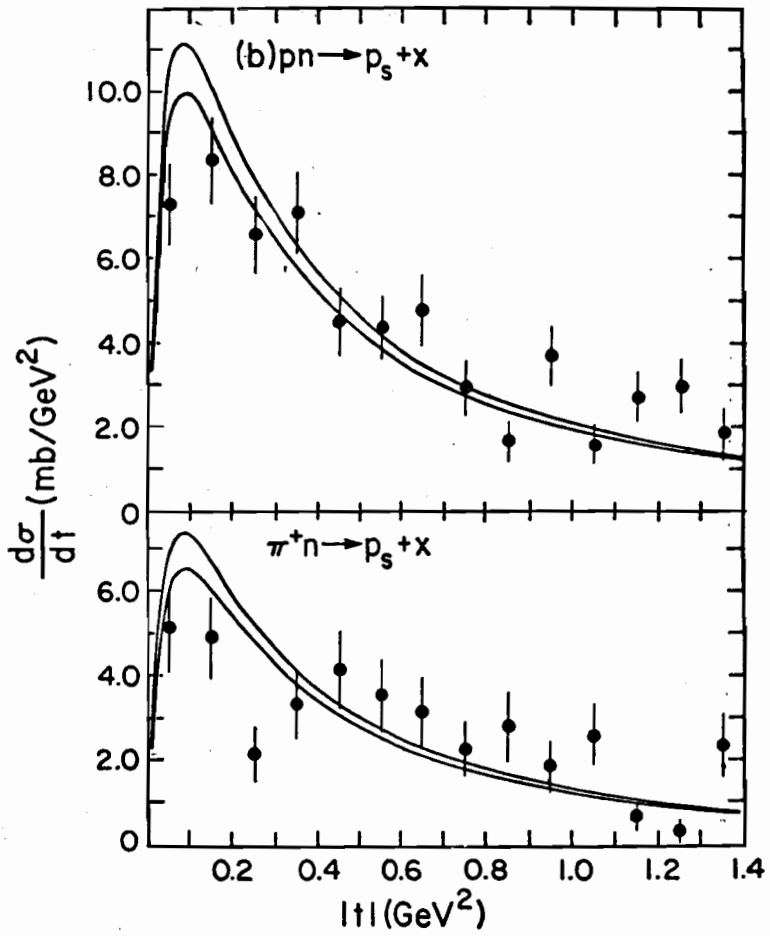
(b)pn→p_s+x
π⁺n→p_s+x
dσ/dt (mb/GeV²)
|t| (GeV²)

Fig. 4b

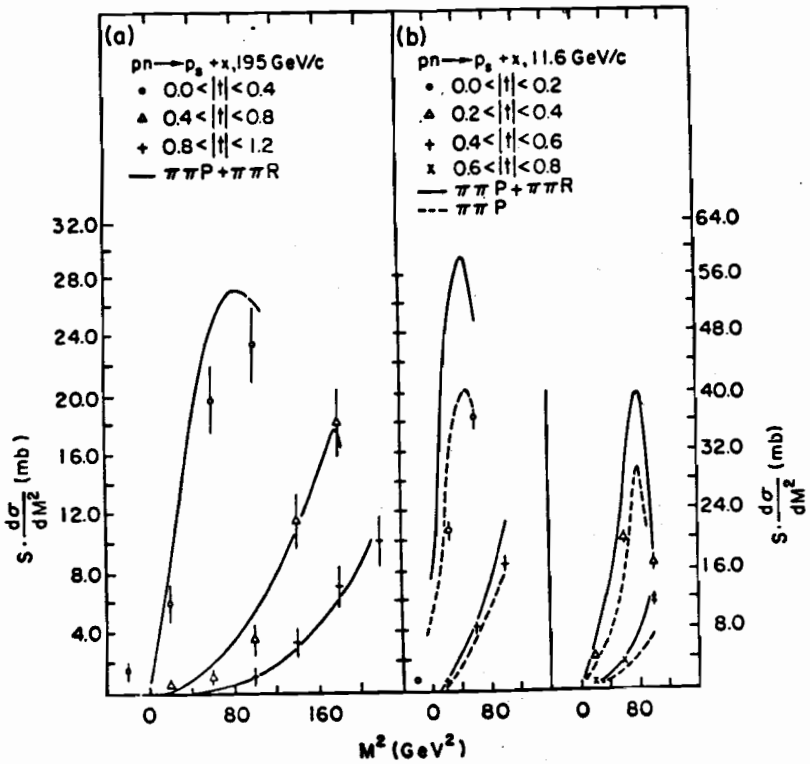
(a)
pn→p_s+x, 19.5 GeV/c
0.0<|t|<0.4
0.4<|t|<0.8
0.8<|t|<1.2
ππP+πππR
(b)
pn→p_s+x, 11.6 GeV/c
0.0<|t|<0.2
0.2<|t|<0.4
0.4<|t|<0.6
0.6<|t|<0.8
ππP+πππR
ππP
S·dσ/dM² (mb)
M² (GeV²)

Fig. 5

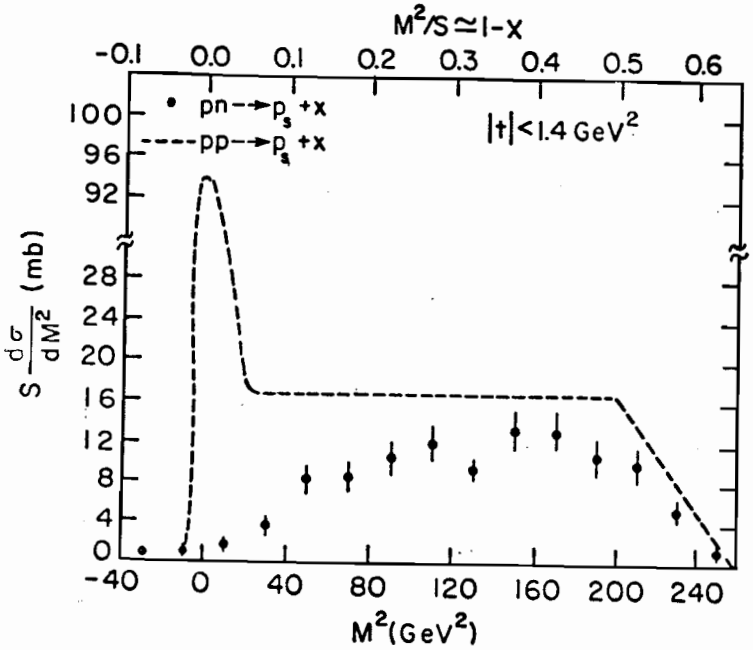
M²/S ≃ 1-X
-0.1 0.0 0.1 0.2 0.3 0.4 0.5 0.6
pn → p_s +x
pp → p_s +x
|t|<1.4 GeV²
S dσ/dM² (mb)
100 96 92 28 24 20 16 12 8 4 0
-40 0 40 80 120 160 200 240
M²(GeV²)

Fig. 6

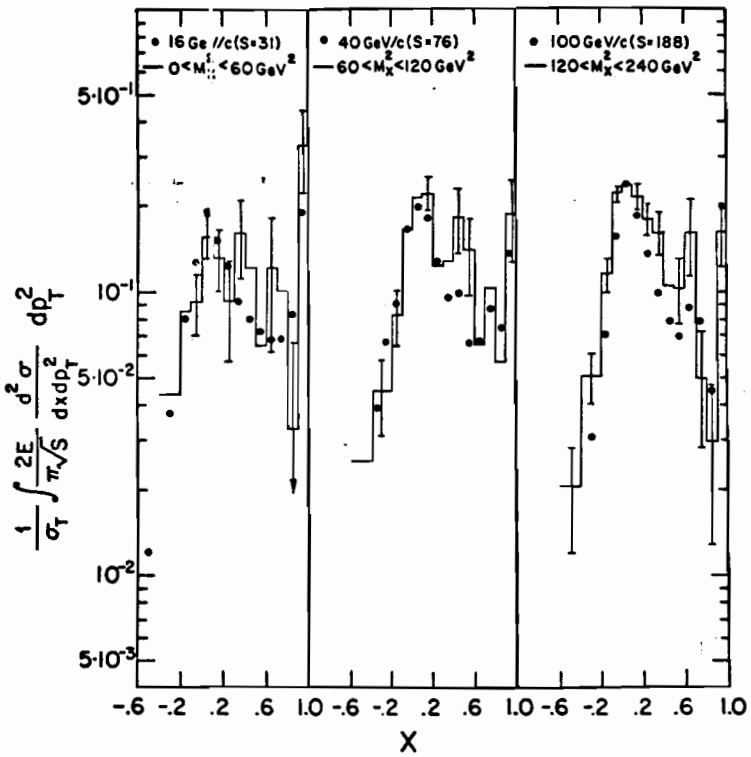
16 GeV/c (S=31)
0<M²_X<60 GeV²
40 GeV/c (S=76)
60<M²_X<120 GeV²
100 GeV/c (S=188)
120<M²_X<240 GeV²
1/σ_T ∫ 2E/√S d²σ/dxdp²_T dp²_T
5·10⁻¹ 10⁻¹ 5·10⁻² 10⁻² 5·10⁻³
-.6 -.2 .2 .6 1.0
X

Fig. 7